Latex migration in battery slurries during drying

Sanghyuk Lim,[†] *Kyung Hyun Ahn,*[†] *and Masato Yamamura**[,‡]

[†]School of Chemical and Biological Engineering, Institute of Chemical Processes, Seoul National University, Seoul 151-744, Korea

[‡]Department of Applied Chemistry, Kyushu Institute of Technology, Kitakyushu, Fukuoka 804-8550, Japan

Abstract

We used real-time fluorescence microscopy to investigate the migration of latex particles in drying battery slurries. The time evolution of the fluorescence signals revealed that the migration of the latex particles was suppressed above the entanglement concentration of carboxymethyl cellulose (CMC), while it was significantly enhanced when CMC fully covered the surfaces of the graphite particles. In particular, a two-step migration was observed when the graphite particles flocculated by depletion attraction at high CMC/graphite mass ratios. The transient states of the nonadsorbing CMC and graphite particles in a medium were discussed, and the uses of this novel measurement technique to monitor the complex drying processes of films were demonstrated.

INTRODUCTION

Suspensions composed of particles and binders are widely used in industry to manufacture a variety of products such as papers,[1] paints,[2] lithium-ion batteries,[3] and solar cells.[4] However, many problems such as delamination,[5] cracks,[6] the coffee stain phenomenon,[7] and print mottle[8] occur during processes such as coating and drying. In particular, the inhomogeneous distribution of particles[9-13] or the binder[14-16] affects film performance such as printability,[9,15] optical properties, adhesion, and others. Therefore, it is important to understand the mechanism of the migration of particles or the binder that occurs during film processing in order to manufacture uniform films.

Some possible underlying physics for particle migration such as capillary flow-induced[17,18] and Brownian motion-induced[10] migrations have previously been suggested. Luo et al.[17] explained that when small clusters of particles pack together by Brownian motion or lateral capillary attraction,[19] a difference in pressure is generated over the curved menisci between the particles, which contacts with air at the top of the film. The resulting capillary-pressure-driven flow induces the migration of particles, and a "top-down" consolidation front[18] separates the particle consolidation layer and dispersed particles in the medium beneath the layer. Zang et al.[10] suggested that latex particles migrate toward the surface of coatings because of the significant amount of Brownian motion among small particles. The small particles are trapped because of interfacial tension associated with a receding air-water interface, leading to a heterogeneous concentration distribution and a high concentration of particles at the surface of the film. On the contrary, Trueman et al.[12] and Nikiforow et al.[13] suggested that slow diffusing larger particles cannot diffuse away from the water/air interface as it drops downwards, resulting in trapping of the larger particles driven by the differences in the particle diffusivity. Although some

hypotheses have previously been proposed for the mechanism of particle migration, the rigorous mechanism is still a subject of ongoing debate.

There have been numerous efforts to understand the mechanism of particle migration, and a variety of measurements have been made. Typical examples include electron spectroscopy for chemical analysis (ESCA),[8,10] ultraviolet analysis,[15,16] cryogenic scanning electron microscopy (Cryo-SEM),[17,18,20,21] and numerical modeling.[20-22] Yamazaki et al.[8] used ESCA to determine the chemical compositions of the surfaces of dried starch/latex composite films and explained that the starch preferentially migrated and affected the print mottle more than the latex did. However, ESCA measurements are limited to the surfaces of dried films. Cryo-SEM, on the other hand, is a powerful tool used to visualize the particle distribution in a cross-section of drying film. This technique involves freezing the specimen in a liquid cryogen to arrest structural changes in the film after it has been dried for a specific amount of time, fracturing the specimen to reveal the coating cross-section, and sputter-coating the fractured specimen to prevent charging before imaging. Cardinal et al.[20] and Buss et al.[21] demonstrated a transient particle distribution in coatings depending on the drying conditions of the films and showed consistency between Cryo-SEM observations and predictions made using a 1D model. However, the sampling rate of the images was relatively limited because of the careful preparation of the samples.[23]

We used fluorescence microscopy (FM) to develop a method for measuring latex particle migration in drying films. Fluorescent latex particles in liquids emit fluorescent light when an excitation laser beam is irradiated through the whole coating. The intensity of the fluorescent light is detected using a microscope, and it provides information on the vertical particle distribution of the coating because the intensity of the florescent light increases as the particle consolidation layer develops in the vicinity of the free surface. FM can be used for measurements

at high sampling rates and can even be applied to opaque and/or thick coatings without any particular preparation necessary for the samples; hence, FM has a great advantage over other measurement techniques.

In this study, we applied FM to drying battery slurries. Li-ion batteries are attracting considerable attention as rechargeable secondary batteries. Extensive efforts have been made to enhance the performance and stability of the Li-ion batteries by using additives,[24] or to enhance the dispersion by adding dispersants,[25] or by changing the methods of coating[3]/mixing.[26] However, little information is known about the transient drying behavior, including particle migration, in battery slurries. It is important to understand the mechanism of particle migration during drying because the particle distribution of dried films would affect the performance and stability of batteries. Therefore, we used FM to investigate particle migration in battery slurries during drying. The experimental setup is presented in Experimental section. In Results section, latex particle migration with and without graphite particles was investigated by varying the concentrations of polymer/graphite under different drying conditions.

EXPERIMENTAL SECTION

Materials

Graphite (SG-BH8, Ito Graphite Co., Ltd., Japan) was used as an active material. The diameter, density, and specific surface area of the graphite particles were 8.1 μm, 2.23 g/cm^3, and 12.12 m^2/g, respectively (provided by manufacturer). Sodium carboxymethyl cellulose (CMC; BSH-6, Dai-ichi Kogyo Seiyaku Co., Ltd., Japan) was used as a thickening agent to prevent sedimentation of the graphite particles.[27] The average molecular weight (M_w) and the degree of substitution of CMC were 290,000–340,000 g/mol and 0.65–0.75, respectively (provided by

manufacturer). Fluorescent polystyrene (PS) particles (micromer®-redF, micromod Partikeltechnologie GmbH, Germany; diameter = 100 nm; density = 1.03 g/cm^3; zeta potential in water = –40 ± 5 mV) were used in this study. The maximum excitation and emission wavelengths of the fluorescent PS particles were 552 and 580 nm, respectively. The fluorescent PS particles were dispersed in water. Hereinafter, the fluorescent PS particles will be called "latex" in this paper.

Preparation method

CMC was dissolved in deionized water and was stirred using a magnetic stirrer for 12 h. The latex suspension was added to the CMC solution and the resulting mixture was mixed for another 12 h. The graphite was added to the latex-CMC suspension and was dispersed using a homogenizer (HG-200, Hsiangtai Machinery Ind. Co., Ltd., Taiwan) with an impeller (K-12S, Hsiangtai Machinery Ind. Co., Ltd., Taiwan) at 10,000 rpm for 3 min. The graphite slurry was mixed for another 12 h. All the samples were prepared just before the experiments. The graphite slurry was prepared for sedimentation and adsorption isotherm measurements in the same manner except that fluorescent latex particles were added to it. The CMC concentrations were chosen to be above 0.4 wt% in order to prevent both lateral heterogeneous particle distribution and sedimentation of graphite particles.

Characterization

A schematic of the drying apparatus is shown in Figure 1a. The intensity of the fluorescent light, the size of the scattered beam, and the solvent mass lost during drying were simultaneously measured. A micropipette was used to coat the specified volume of battery slurry onto the glass

substrate with a stainless steel guide. The diameter and the height of the coating were 56 mm and 500 μm, respectively. A TEM00-mode laser (Lasiris™ Green, Coherent, Inc., USA; wavelength = 532 ± 1 nm) whose beam intensity obeyed a single Gaussian distribution was held in position at a 45° incidence to the coating. The laser intensity was adjusted using a neutral density (ND) filter to avoid a saturation of fluorescence images. Lasers whose intensities were 110 μW, 1.17 mW, and 7.12 mW were used to irradiate the coatings for graphite-free, 1 wt%, and 5 wt% graphite slurries, respectively. A charge-coupled device (CCD) color camera system (VB-7010, Keyence Co., Ltd., Japan) with a band-pass filter (580 ± 5 nm) was used to capture the emission signals from the fluorescent PS particles. The maximum intensity of the Gaussian distribution with respect to the background value was analyzed using software (VH analyzer, Keyence Co., Ltd., Japan) and was used as the characteristic intensity of the fluorescent light used in this study (Figure 1b). A CCD beam profiler (Beam On, Duma Optronics, Ltd., Israel) was located on the opposite side of the laser at a 45° reflection, and it was used to capture the size and shape of the laser beam reflected from the coating. The image captured by the CCD beam profiler was analyzed using software (Beam On USB 2.0 measurement system, Duma Optronics, Ltd., Israel), as shown in Figure 1c. The drying temperature of the film was adjusted using a micro warm plate (MD-10DMFH, Kitazato Co., Ltd., Japan) located beneath the coating at interspaces of 250 μm to uniformly heat the bottom of the coating. Solvent loss was simultaneously measured using an electronic balance (Cubis® MSE-3203S-0-00-DE, Sartorius Mechatronics Japan, K.K., Japan) during drying. All equipment was set up on a vibration isolator (TDI-129-100LM, Sigma Koki Co., Ltd., Japan) and was covered with a black curtain to prevent outside light from interfering with the measurements.

Images of the surface of the dried film were captured using an optical microscope (x500; VH-Z100R, Keyence Co., Ltd., Japan) and an atomic force microscope (Nanopics 2100, SII Nano Technology, Inc., Japan) in noncontact mode. In addition, a cross-section of the dried film was taken using field-emission scanning electron microscopy (FE-SEM, JSM-6320F, JEOL, Ltd., Japan). The specimen used for FE-SEM was fractured after it was immersed into liquid nitrogen to cleanly cut the specimen.

The viscosity of the CMC solution was measured using a strain-controlled rheometer (ARES, TA instruments) with a 50 mm-diameter cone and plate fixture and a stress-controlled rheometer (AR-G2, TA instruments) with a 40 mm-diameter cone and plate fixture.

Isotherms for the amount of CMC adsorbed onto graphite were measured as functions of CMC concentration. Graphite slurries containing 5 wt% graphite and various concentrations of CMC were prepared, and the supernatant was extracted after the slurries were centrifuged at 50,000 rpm until graphite particles had completely separated from the supernatant. The amount of CMC adsorbed onto the graphite was calculated by determining the concentration of nonadsorbing CMC in the supernatant.

A sedimentation test was performed on graphite slurries without added latex particles. Graphite slurries containing various concentrations of CMC were prepared using the same method and were kept in a container on a vibration isolator for 2 weeks.

[ISERT **Figure 1.**]

RESULTS

Validation of intensity of fluorescent light

Validation tests were performed to investigate the relation between the intensity of the fluorescent light emitted from the samples and the mass fractions of fluorescent particles in the samples.[28] The tests were performed in a darkroom at room temperature and 29% relative humidity. Figure 2a indicates the relation between the initial intensity of the fluorescent light and the coating height for various concentrations of latex particles. The intensity of the fluorescent light monotonically increased with coating height at the initial drying stage and also increased more rapidly with increasing latex concentration. The intensity of the fluorescent light emitted for each coating height was normalized using the intensity of fluorescent light emitted from the same height of a coating containing 0.1 wt% latex particles (Figure 2b). The normalized intensity of fluorescent light showed a power law relation with latex concentration (power law exponent of 0.86), indicating that the present measurements of the intensity of fluorescent light enable us to determine the local concentrations of latex particles in drying films.

[ISERT **Figure 2.**]

Latex migration in polymer solution

Before we investigated the mechanism of latex migration in graphite slurries, we studied latex migration in a polymer solution containing 0.4 wt% latex particles dried at various drying temperatures. The intensity of the fluorescent light emitted is shown as functions of drying time for CMC concentrations of 0.5 (Figure 3a) and 1.0 wt% (Figure 3b). The intensity of the fluorescent light emitted during drying was normalized using the initial fluorescence intensity, F_0. The drying time was described as dimensionless time, $t_D = (t_r \cdot E)/H_0$, where t_r, E, and H_0 denote

the drying time, initial evaporation rate in units of velocity, and initial coating height, respectively.

The development of the intensity of the fluorescent light showed complex behavior depending on CMC concentration and drying temperature. The intensity of the fluorescent light emitted from the 0.5 wt% CMC solution first decreased toward the minimum value during the initial drying stage (regime I), increased to a maximum (regime II), and eventually decreased dramatically toward the final value during the late drying stage (regime III), as shown in Figure 3 (c). The minimum intensity of fluorescent light decreased with increasing drying temperature, whereas the maximum and final intensities of fluorescent light increased. The transition from regime II to III was found to shift to a longer drying time as the drying temperature increased.

For the 1.0 wt% CMC solution, on the other hand, the intensity of the fluorescent light emitted from the solution dried at 30°C remained constant until it finally decreased below unity. In addition, the maximum and final intensities of fluorescent light were independent of drying temperature at 50 and 70°C.

[ISERT **Figure 3.**]

The interfacial structure on the suspension surface may affect the concentration-dependent evolutions of fluorescence. To check this, we measured the developments of the beam spot reflected from the air-liquid interface at 30°C for coatings of 0.5 (Figure 4) and 1.0 wt% CMC (Figure 5). The profile of the beam spot was elliptical during initial drying but became more scattered during drying. We monitored the vertical and horizontal widths of the beam spot, corresponding to the parallel and perpendicular directions of laser reflection, respectively. Both

the vertical and horizontal widths of the beam spot decreased during initial drying (a→b in Figure 4). The horizontal width of the beam spot then increased (b→c in Figure 4), whereas the vertical width of the beam spot slightly increased during drying, indicating an anisotropic beam profile. As drying progressed further, both the vertical and horizontal widths of the scattered beam drastically increased at $t_D \approx 0.9$ (c→d in Figure 4) and eventually reached a constant. Interestingly, t_D is consistent with the time at which we observed the transition between regimes II and III in FM. In contrast, the beam spots obtained for the 1.0 wt% CMC solution maintained their shape and size (a→b in Figure 5) and then gradually increased (b→c→d in Figure 5), showing a different development in the size of the beam spot depending on the concentration of CMC.

[ISERT **Figure 4.**]

[ISERT **Figure 5.**]

Latex migration in graphite slurry

To elucidate how fluorescence changes by adding graphite particles to the latex-CMC suspension, we conducted drying experiments for graphite slurries containing various concentrations of graphite and CMC and at various drying temperatures. Figure 6 indicates the fluorescence developments for 1 and 5 wt% graphite slurries containing 0.4 wt% latex particles and 0.7 wt% CMC, compared with the graphite-free system at 70°C. When 1 wt% graphite was added to the suspension, intensity of the fluorescent light first decreased during initial drying similar to graphite-free systems and then increased to a great extent at approximately 0.25 of

dimensionless time followed by a second similar increase in intensity up to $F/F_0 \approx 3.5$ when the normalized time is 1.5. However, the intensity of the fluorescent light emitted from the 5 wt% graphite slurry decreased and followed the behavior of graphite-free solutions until the dimensionless drying time of $t_D = 1.4$, where the fluorescence showed a weak peak. And then, the intensity of the fluorescent light emitted from the 5 wt% graphite slurry then gradually decreased. To understand the different trends in the intensity of the fluorescent light depending on the concentration of graphite, we directly visualized segregation of latex particles on the surface of the dried coating. Figures 7a–c and 7d–f indicate the images for 1 and 5 wt% graphite slurries, respectively, under the same drying conditions as the slurries shown in Figure 6. Because latex particles emit a weak fluorescence under the light for optical microscopy, the bright domains in Figure 7a represent the segregated latex particles distinguishable from optically dark graphite layers. As shown in the optical microscope and atomic force microscope images, the segregated latex particles appeared on the surface of 1 wt% graphite slurry (Figures 7a and 7b), while there was no distinct segregation of latex particles on the surface of 5 wt% graphite slurry (Figures 7d and 7e). In addition, cross-sectional imaging revealed that the latex particles had segregated above the graphite consolidation layer for the 1 wt% graphite slurry (Figure 7c), while they seemed to be well-dispersed among the graphite particles for the 5 wt% graphite slurry (Figure 7f). Although the optical and atomic force microscopy images were not taken at the same position of the samples, different regions of each surface were imaged to ensure that a representative image was obtained.

[ISERT **Figure 6.**]

[ISERT **Figure 7.**]

In the second series of experiments, the CMC concentration and drying temperature were varied, while the graphite concentration was maintained at 5 wt% (Figure 8). The intensity of the fluorescent light emitted from the slurry dried at a low drying temperature of 30°C remained constant at approximately unity during initial drying (Figure 8a), whereas it slightly increased with time at higher CMC concentrations (Figure 8b). On the contrary, the intensity of the fluorescent light emitted from the slurry dried at 70°C decreased with time during initial drying at both CMC concentrations, as observed for the graphite-free system. The maximum and final intensities of the fluorescent light emitted from the 0.5 wt% CMC slurry increased with increasing drying temperature (Figure 8a), while those of fluorescent light emitted from the 1.0 wt% CMC slurry were independent of drying temperature, showing a similar intensity development as that of the graphite-free system. It is worth noting that the graphite slurries containing 1.0 wt% CMC exhibited much smaller variations in the intensity of the fluorescent light emitted than those containing 0.5 wt% CMC.

[ISERT **Figure 8.**]

DISCUSSION

As shown in [Latex migration in polymer solution] section in the RESULTS, the drying stages could be subdivided into three regimes on the basis of the development of the intensity of the fluorescent light emitted from the sample and from the size of the beam spot. In this section, the

time evolution of the intensity of the fluorescent light is discussed in the light of the migration and packing of latex particles in the vicinity of the air-liquid interface.

Evolution in particle consolidation layer

First, let us consider the variation in the refractive indices of the suspensions. The refractive indices of air (n_{air}), water (n_{water}), and polystyrene (n_{ps}) are 1.00026,[29] 1.33585,[30] and 1.59861,[31] respectively. The latex particles were well dispersed throughout the medium during initial drying. As water evaporated during drying, the latex particles are accumulated at the top surface of the coating because of their slow diffusion and became closer to each other, leading to an increase in the refractive index of suspension. According to Snell's law, this leads to a decrease in the refraction angle at the free surface. These facts are consistent with our simultaneous fluorescence/beam-size measurements in drying regime I in which the size of the reflected beam spot decreased to a minimum, indicating that initial particle packing proceeds in this regime.

In regime II, the latex particles subsequently formed a consolidation layer at the top surface of the coating. The lower liquid pressure beneath the curved meniscus in the consolidation layer initiated capillary pressure-induced flow, which, in turn, accumulated the particles beneath the layer. As the consolidation layer thickened, the consolidating particles emitted more fluorescent light, thereby overcoming the decrease in the intensity of the fluorescent light owing to the variation in the refractive index. This finding is consistent with the increase in the intensity of the fluorescent light emitted from the suspension containing higher concentrations of latex particles, as shown in Figure 2.

The formation of a consolidation layer on top of the coating can be explained in terms of the dimensionless Peclet number (Pe) and the sedimentation number (N_s), which represent the

balance among the evaporation, diffusion, and sedimentation of particles.[20,21] The dimensionless Peclet number is defined as

$$Pe = (E \cdot H_0) / D_0, \quad (1)$$

where E is the evaporation rate of the solvent, H_0 is the initial coating height, and D_0 is the Stokes-Einstein diffusion coefficient, which is defined as

$$D_0 = kT / 6\pi\mu R, \quad (2)$$

where k is the Boltzmann constant, T is the drying temperature, μ is the viscosity of the medium, and R is the radius of the particle. The Peclet number represents a balance between the evaporation and diffusion of particles in the medium.

The sedimentation number can be defined to describe the balance between sedimentation and evaporation as

$$N_s = U_0 / E, \quad (3)$$

where U_0 is the Stokes' settling velocity, which is given as

$$U_0 = 2R^2 g(\rho_P - \rho_L)/9\mu, \quad (4)$$

where g is the gravitational acceleration, $\rho_P - \rho_L$ is the difference between the particle density (ρ_P) and the density of the dilute solution (ρ_L), and μ is the viscosity of the polymer solution.

Evaporation is dominant, and a discontinuous particle distribution forms in films for which $Pe \gg 1$.[20-22] In contrast, a homogeneous particle distribution evolves under a diffusion dominant condition of $Pe \ll 1$. In addition, when $N_s \ll 1$, the sedimentation does not occur. The particle distributions in water[20] and in the polymer solution[21] during drying have previously been

predicted based on dimensionless numbers such as Pe and N_s. When the latex suspension composed of 0.5 wt% CMC was dried at 30°C, the estimated Peclet and sedimentation numbers were 4.05×10^3 and 5.88×10^{-6}, respectively (Table 1). The results modeled by Buss et al.[21] revealed that the critical Peclet number, at which the evaporation- and diffusion-dominant regions can be separated, is approximately $Pe_c = 0.63$ for a suspension containing 10 vol% of particles and 1 vol% of polymer, suggesting that a consolidation layer forms early during drying under the present conditions of $Pe >> Pe_c$ and $N_s << 1$. In addition, our preliminary numerical simulation based on the previous model by Cardinal et al.[20] demonstrated that a consolidation layer formed during initial drying (not shown here), although we simply ignored the polymer effect that occurred during drying because of the lack of information on the diffusion coefficient of CMC.

[ISERT **Table 1.**]

Further evidence as to the formation of a consolidation layer is also supplied by our beam spot measurements. When a laser beam was irradiated into a consolidation layer, the beam was diffracted or even scattered by closely packed particles and showed a broader spot as the layer thickened during evaporation. This finding is consistent with our observation that the beam reflected from the coating surface exhibited an increase in its spot size as the drying proceeded in regime II (b→c in Figure 4). It is worth noting that the consolidation layer in this regime was saturated with water so that the mass-loss curves exhibited a constant slope (Figure 3a).

As water further evaporated, the air-water interface began to recede toward the bottom of the surface, and the consolidation layer protruded above the air-water interface.[32] This stage, defined

as regime III in this study, is usually referred to as a falling rate period, in which the rate of solvent loss begins to decrease beyond the end of the constant rate period. The protruded consolidation layer gives rise to an increase in the amount of emitted lights scattered due to invaded air into the voids among particles. Indeed, our beam profile measurements revealed that the elliptic reflected beam began to collapse because of strong beam scattering and showed a drastic increase in beam spot size at the onset of the falling rate period (c→d in Figure 4). As a result, the intensity of the fluorescent light emitted from the suspension suddenly decreased to the final intensity (Figure 3a). These findings strongly suggest that the consolidation layer on the top surface protruded into the air as the air-water interface receded and that the air invaded into the pores among the particles, replacing water during the falling rate period. The measured temporal fluctuations in the intensity of the scattered light might allow us to determine the average mean-square displacement of the scattering particles [33] and viscoelastic behavior [34] of the suspension by applying the theory for diffusing wave spectroscopy and speckle interferometry.[35,36] However, the direct application of the scattering theory is beyond the scope of this study.

To further prove the particle consolidation formation, we estimated the overall fluorescent intensities in the auto-stratified latex suspension by utilizing the calibration curve, and compared them with experimental data. Previous numerical studies have shown that all latex particles are trapped in the consolidation layer at sufficiently high Pe, giving rise to a discontinuous particle concentration profile in the thickness direction[22], and hence, the thickness of the particle consolidation layer on top of the coating can be obtained from a mass balance of the particle. Substituting the estimated consolidation layer thickness and the light absorption coefficient of the latex particle into the Lambert-Beer law allows us to estimate the overall intensity of

excitation light absorbed in the consolidation layer. Multiplying the quantum yield of the latex particle, we estimated the "averaged" fluorescent intensity from the particle consolidation layer as well as the intensity from the bottom layer. Because a part of the fluorescence light from the bottom layer is absorbed in the consolidation layer, the resultant overall fluorescent intensity strongly depends on how the particles are stratified in the suspension. Considering a random closed packing of latex particles with a particle volume fraction of 0.64, the estimated maximum dimensionless fluorescent intensity (F/F_0) was 1.1 at 30°C, showing a good agreement with the corresponding experimental value shown in Figure 3a.

Suppressed migration in dense CMC solution

To address the suppressed latex migration, we next focused on entanglements of CMC chains. CMC molecules form a polymeric network and show a gel-like behavior when they are above a critical concentration.[37] Furthermore, CMC tends to form different molecular conformations such as extended chains, coiled chains, and gels, depending on CMC concentration.[38] The critical concentration of CMC can be obtained from the relation between the solution viscosity and the concentration of the polymer.[39,40] The polymer solution can be divided into three regimes by two critical concentrations: c^*, defined as an overlap concentration, and c_e, defined as an entanglement concentration such that: i) a dilute regime occurs where $c < c^*$, ii) a semidilute unentangled regime occurs where $c^* < c < c_e$, and iii) a semidilute entangled regime occurs where $c_e < c$.[40,41] In the dilute regime, CMC is freely dispersed throughout the medium below c^*. As the concentration of CMC increases above the overlap concentration, c^*, the polymer chains begin to overlap. The c^* was determined from the inverse of the intrinsic viscosity, *i.e.*, $c^* \approx 1/[\eta]$. We estimated the intrinsic viscosity of CMC solution not only experimentally using the

Huggins (Eq. 5)[42] and Kraemer equations (Eq. 6)[43] but also theoretically using the Mark-Houwink equation:

$$\eta_{sp} / c = [\eta] + k_H[\eta]^2 c, \quad (5)$$

$$(\ln \eta_{rel}) / c = [\eta] - k_K[\eta]^2 c, \quad (6)$$

where η_{sp} is the specific viscosity (= η/η_0–1), η_{rel} is the relative viscosity (= η/η_0), c is the concentration of polymer, and k_H and k_K are the Huggins and Kraemer constants, respectively.

Fitting the viscosity measurements gave $[\eta]$ = 74.94 dl/g, determined as the y-intercept of both the Huggins (open circle) and Kraemer (closed circle) relation, where k_H and k_K are 1.317×10^{-1} and 4.004×10^{-2}, respectively (Figure 9a).

In addition, the intrinsic viscosity of CMC was determined as 49.84 dl/g from the Mark-Houwink equation:

$$[\eta] = KM^a, \quad (7)$$

where K was the Mark-Houwink constant (0.1×10^{-5} dl/g) and the exponent, a, was 1.4 (for an aqueous 0.001 M NaCl).[44]

The intrinsic viscosity (49.84 dl/g) obtained using the Mark-Houwink equation was slightly different from the experimentally obtained one (74.94 dl/g) because it was difficult to accurately measure the viscosity of low concentrations of CMC with a rotational rheometer. From the values of intrinsic viscosity, c^* was estimated in the range 0.013–0.02 g/dl.

As the concentration of CMC further increased, the semidilute regime of CMC changed from the semidilute unentangled into the semidilute entangled regime through an entanglement concentration, c_e.[40] The entanglement concentration was obtained by the relation between the viscosity and the concentration of CMC as $\eta \sim c^n$. Although the viscosity of CMC slightly

increased with increasing CMC concentration in the semidilute unentangled regime (n = 1.17), it dramatically increased with n = 4.20 in the semidilute entangled regime (Figure 9b). The slopes of the log η–log concentration of CMC plots for both regimes coincided with those from previous work, as the exponents for a linear polymer in a good solvent were 1.25 and 4.25–4.5 for the semidilute unentangled and semidilute entangled regimes, repectively.[40,45-47] Therefore, the entanglement concentration for CMC was obtained as c_e = 0.56 wt% at the onset of the semidilute entangled regime, which implies that the migration of latex particles in the 1.0 wt% CMC solution was significantly suppressed because of the entanglements of CMC. The latex particles in the 0.5 wt% CMC solution, on the other hand, could freely migrate during drying because the CMC polymers did not form entanglements at that concentration.

[INSERT **Figure 9.**]

This finding is consistent with our observation that the intensity of the fluorescent light (Figure 3b) and the size of beam spot (Figure 5) for suspension containing the high concentration (1.0 wt%) of CMC were independent of dimensionless time at drying temperature of 30°C. Indeed, there have been some previous reports that migration of latex particles was suppressed by water-soluble polymers such as CMC[10,48] and starch.[9] According to the reports, the migration of latex particles was inhibited either by the bridging structure between the latex and pigment particles or by the network structure of the polymers. In addition, it became more difficult for water molecules to penetrate into the three dimensional network of CMC because of the high density of CMC chains.[49] Therefore, the latex particles were trapped, retaining their distribution in the entanglements as water evaporated and the coating shrank, and the well-packed distribution of

the latex particles was finally formed in the coating.

As a result, the microstructure of the latex in the coating for two different CMC concentrations can be inferred by the development of the intensity of the fluorescent light emitted from the suspension and from the sizes of the beam spots. The latex particles were well dispersed throughout the CMC solution during initial drying regardless of the CMC concentration (Regime I). However, the "top-down" consolidation appeared in the solution containing a low concentration of CMC, in which the consolidated layer of latex particles at the top coexisted with the dispersed particles beneath the layer in the coating (Regime II) followed by the invasion of the air-liquid interface into the coating (Regime III). The motion of the latex particles in the solution containing a high concentration of CMC, on the other hand, was hindered by the entanglement of the CMC. Therefore, nonuniform distribution of latex particles in the film would be expected to form for low concentrations of CMC, while uniform distribution of latex particles would be expected to form for high concentrations of CMC.

Not only the CMC concentration but also the drying temperature affected the migration of latex particles during drying. The Stokes-Einstein diffusion coefficient, D_0, increased with increasing drying temperature because of the decrease in the viscosity of the polymer solution. Although D_0 increased with increasing drying temperature, *Pe* increased because the extent of the increase in the evaporation rate was larger than that of the increase in the diffusion coefficient. In addition, the sedimentation number, N_s, decreased with increasing drying temperature (Table 1). Therefore, the migration of latex particles was enhanced by high *Pe* and low N_s at high drying temperatures, which is consistent with the increase in the maximum and final intensities of fluorescent light emitted from the suspension containing a low concentration of CMC as increasing drying temperature (Figure 3a).

Accelerated migration in graphite slurries

The bimodal graphite slurries showed different evolutions in the migration of latex particles, *i.e.*, the migration of latex particles was accelerated by the addition of graphite particles (see Figure 6). Let us consider a particular case in which the graphite and latex particles co-consolidate at the top surface. The smaller latex particles fill in the space among the graphite particles, and capillary-driven convective flow transports latex particles through the pore throat to the evaporating menisci.[17] As drying progresses, the capillary pressure gradient increases and draws more latex particles into in the consolidation layer where they become trapped, eventually resulting in a latex-rich zone at the surface. Indeed, the Peclet and sedimentation numbers estimated based on the diameter of graphite particles were $Pe = 5.62 \times 10^5$ ($>> Pe_c$) and $N_s = 6.34 \times 10^{-1}$ for 0.5 wt% CMC at drying temperature of 70°C, implying that both graphite and latex particles co-consolidate through evaporation-dominant migration without any gravity-driven settling. Furthermore, we estimated the pore-throat diameter by simply assuming a hexagonal particle packing in which the ratio of the radius of the pore throat to the radius of the particle was about 0.15. The estimated throat diameter was found to be 1.2 μm, big enough to enable the latex particles to pass through the space. However, this physical picture is insufficient to explain why more latex particles migrate at the intermediate graphite concentration of 1 wt%. To gain deeper insight, we focused on CMC adsorption onto graphite surfaces and the corresponding variations in the interparticle forces in graphite slurries.

Figure 10 indicates the isotherms for CMC adsorption onto graphite particles in slurries containing 5 wt% graphite and various concentrations of CMC. The amount of CMC that

adsorbed onto the graphite particles increased with increasing CMC concentration and saturated at 0.9 mg/m^2 above the critical concentration of 0.4 wt%, indicating that CMC had fully covered the graphite surface and that nonadsorbed polymers remained in the medium above the critical CMC/graphite mass ratio, r_c = 0.08.

[INSERT **Figure 10.**]

CMC adsorption significantly affects the stability of slurries or suspensions.[50-52] Figures 11(a) and 11(b) indicate the sedimentation trends for slurries composed of 5 wt% graphite and various concentrations of CMC and for those composed of 1 wt% graphite and 0.7 wt% CMC, respectively.

At low CMC/graphite mass ratios less than r_c, the graphite particles settled among adsorbing polymers by either gravity or bridging flocculation.[53-55] As the concentration of the polymer increased above r_c, the polymer fully covered the surfaces of the particles, and the slurry stabilized through steric repulsion (Figure 11a).[52] The graphite particles resettled with a further increase in the concentration of the polymer, and the supernatant and graphite particles in the solution containing 1 wt% graphite and 0.7 wt% CMC (*i.e.*, the solution with a CMC/graphite mass ratio of 0.7) were completely separable (Figure 11b). A depletion flocculation occurred by nonadsorbed polymer.[56-58] As the particles moved closer to each other, the polymer located among the particles became excluded to the outside of the particles. The resulting difference in the concentration between in the bulk medium and in the overlap region among the particles promoted higher osmotic pressure in the bulk medium than in the overlap region, and induced flocculation of the particles.[59] When the graphite particles were flocculated, the curved menisci

between the flocculated particles pulled the fluid to the surface because of capillary force, and, hence, the latex particles could easily migrate through the path between the flocculates toward the free surface, leading to a thicker consolidation layer at the top surface. This finding is consistent with the highest intensity of fluorescent light (Figure 6) emitted from the suspension and with the segregation of latex particles on top of the graphite consolidation layer (Figure 7c) for the 1.0 wt% graphite slurry containing 0.7 wt% CMC. As the water evaporated, the latex particles co-consolidated with the graphite particles and migrated through the pore throats among the graphite particles and toward the coating surface, leading to an increase in the intensity of the fluorescent light emitted. The segregated latex particles protruded into the air and then the curved menisci among the latex and graphite particles pulled the fluid further upward, giving rise to the second increase in the intensity of fluorescent light during late evaporation. This physical picture is consistent with the two-step development in the intensity of the fluorescent light emitted from the slurry (Figure 6). For the 5 wt% graphite slurry whose CMC/graphite mass ratio, $r = 0.12$, on the other hand, steric forces among polymers adsorbing onto the surfaces of graphite particles pushed the graphite particles apart producing longer interparticle distances and possibly giving rise to weaker capillary forces and thus less migration of latex particles.

[INSERT **Figure 11.**]

Figure 12 summarizes the transitions in the minimum, maximum, and final intensities of the fluorescent light emitted from the samples with respect to CMC and graphite concentrations, taking into account the entanglements of neighboring CMC chains and CMC adsorption onto graphite particles.

As shown in Figure 12a, the minimum intensities of the fluorescent light emitted from the graphite-free suspension remained constant at approximately 0.9 and then increased with increasing concentration of CMC to 1.0 wt%. The minimum intensity of fluorescent light indicated the dispersion state of latex particles during initial drying, regime I, before forming a consolidation layer on the top surface of the coating. While the latex particles in the CMC solution containing a low concentration of CMC are diffused toward the air-water interface of the coating, the migration of latex particles was suppressed by CMC entanglement in the solution containing a high concentration of CMC. The distribution of latex particles was almost unchanged so as to show the minimum intensity (i.e., unity) of fluorescent light. The minimum intensity of fluorescent light emitted from the 5 wt% graphite slurry, on the other hand, remained constant regardless of the concentration of CMC.

The maximum intensity of fluorescent light emitted from the samples represented the formation of a consolidation layer during drying (Figure 12b). The intensity of the fluorescent light increased with the accumulation of latex particles in the consolidation layer during the drying stage in regime II. The maximum intensity of the fluorescent light emitted from the graphite-free suspension decreased and remained at unity with increasing CMC concentration. At low CMC concentrations, the latex particles could easily migrate toward the consolidation layer through capillary flow induced by the consolidated particles. However, as the CMC concentration increased, the migration of latex particles was suppressed by the entanglement of CMC, resulting in an intensity of unity for the fluorescent light emitted from the samples. On the contrary, the maximum intensity of the fluorescent light emitted from the 5 wt% graphite slurry was much higher than that emitted from the graphite-free suspension because of the strong capillary effect. In our bimodal graphite/latex slurries, the neighboring latex-latex, graphite-latex,

and graphite-graphite particles on the free surface form the throats, which induce the capillary pressures being inversely related to the radius of the throats. Although the capillary pressure difference created by the throat between the larger graphite particles is lower than that by the latex particles, the addition of graphite particles into the latex suspensions leads to an increase in the total particle volume fractions, and thus the number of throats between the particles. Therefore, more latex particles could migrate to the consolidation layer in the graphite slurry, showing a stronger effect of capillary force compared to the graphite-free suspensions. In addition, at around the critical ratio of CMC/graphite, r_c, the graphite particles were well dispersed in the medium because of the steric repulsion induced by adsorbed CMC. As a result, the graphite particles were separated from each other by steric hindrance, and the latex particles could migrate through the space among the graphite particles. However, the migration of latex particles was disturbed by nonadsorbing CMC above r_c, resulting in a decrease in the maximum intensity of fluorescent light with increasing CMC concentration above r_c.

The final intensity of the fluorescent light emitted from the samples represented the structure of the dried film (Figure 12c). The intense fluorescent light emitted from the dried film of 5 wt% graphite slurry implied that more latex particles were distributed on top of the surface of the slurry than the dried film of the graphite-free suspensions, showing a trend similar to that of the maximum intensity.

[INSERT **Figure 12.**]

CONCLUSIONS

Migration of latex particles in drying CMC solution and graphite slurries during drying was investigated using FM, enabling us to determine the development of vertical particle distribution in coatings by analyzing the development of the intensity of the fluorescent light emitted from the samples.

The development of the intensity of the fluorescent light represented the migration of latex particles during drying. The intensity of the fluorescent light decreased during initial drying, regime I, indicating that the latex particles were dispersed throughout the medium. As the water further evaporated, a consolidation layer was formed on the top surface of the coating, and the latex particles accumulated in that layer through capillary pressure-induced flow, leading to an increase in the intensity of the fluorescent light during this stage, regime II. The intensity of the fluorescent light dramatically decreased because of the strong scattering from the protruded consolidation of latex particles at the onset of the falling rate period in regime III, indicating that the air-water interface invaded into the consolidation layer. The intensity of the fluorescent light was independent for high concentrations of CMC, on the other hand, indicating that the migration of latex particles was suppressed by CMC molecules. The CMC chains showed different states such as dilute, semidilute unentangled, and semidilute entangled in the medium depending on the concentration of CMC with respect to two critical concentrations, overlap and entanglement concentrations. The CMC formed entanglements above the entanglement concentration, so the migration of latex particles was interrupted by CMC chains. Therefore, latex particles were more uniformly distributed throughout films produced with high concentrations of CMC, while it were nonuniformly distributed throughout films produced with low concentrations of CMC.

The CMC chains adsorbed onto the surfaces of the graphite particles, and the microstructures formed from the graphite particles and CMC were dependent upon the amount of adsorbed CMC. The microstructures of the graphite slurry affected the migration of latex particles during drying. The graphite particles aggregated because of depletion attraction by nonadsorbed CMC when the mass ratio of CMC/graphite was large, so there was sufficient space among the aggregation of graphite particles to enable the latex particles to migrate and segregate. When the mass ratio of CMC/graphite was close to r_c, on the other hand, the graphite particles maintained a stable structure because of steric repulsion, and the latex particles neither migrated nor segregated.

This study shows that the migration of latex particles is significantly affected by the microstructures that form in graphite slurries. Thus, the microstructures formed by graphite and CMC in slurries should be studied in more detail to determine the drying mechanism of graphite slurry which shows diverse and complicated film structure.

AUTHOR INFORMATION

Corresponding Author

*E-mail: yamamura@che.kyutech.ac.jp.

Notes

The authors declare no competing financial interest.

ACKNOWLEDGMENT

This work was supported by the Japan Society for the Promotion of Science (JSPS) KAKENHI (23560912) Grant-in-Aid for Scientific Research C and the National Research Foundation (NRF) of Korea grant (No. 20100026139) funded by the Ministry of Education, Science, and Technology (MEST).

REFERENCES

(1) Bemada, P.; Bruneau, D. Drying of a Paper Coating: Experimental Study and Modelling. *Dry. Technol.* **1997**, 15, 2061-2087.

(2) Cohu, O.; Magnin, A. Rheometry of Paints with regard to Roll Coating Process. *J. Rheol.* **1995**, 39, 767-785.

(3) Dominko, R.; Gaberscek, M.; Drofenik, J.; Bele, M.; Pejovnik, S.; Jamnik, J. The Role of Carbon Black Distribution in Cathodes for Li Ion Batteries. *J. Power Sources* **2003**, 119–121, 770-773.

(4) O'Regan, B.; Grätzel, M. A Low-Cost, High-Efficiency Solar Cell Based on Dye-sensitized Colloidal TiO_2 Films. *Nature* **1991**, 353, 737-740.

(5) Sarkar, A.; Tirumkudulu, M. S. Delamination of Drying Nanoparticle Suspensions. *Soft Matter* **2011**, 7, 8816-8822.

(6) Tirumkudulu, M. S.; Russel, W. B. Cracking in Drying Latex Films. *Langmuir* **2005**, 21, 4938-4948.

(7) Deegan, R. D.; Bakajin, O.; Dupont, T. F.; Huber, G.; Nagel, S. R.; Witten, T. A. Capillary Flow as the Cause of Ring Stains from Dried Liquid Drops. *Nature* **1997**, 389, 827-829.

(8) Yamazaki, K.; Nishioka, T.; Hattori, Y.; Fujita, K. Print Mottle Effect of Binder Migration and Latex Film Formation during Coating Consolidation. *Tappi J.* **1993**, 76, 79-84.

(9) Du, Y.; Zang, Y. H.; Du, J. Effects of Starch on Latex Migration and on Paper Coating Properties. *Ind. Eng. Chem. Res.* **2011**, 50, 9781-9786.

(10) Zang, Y. H.; Du, J.; Du, Y.; Wu, Z.; Cheng, S.; Liu, Y. The Migration of Styrene Butadiene Latex during the Drying of Coating Suspensions: When and How Does Migration of Colloidal Particles Occur?. *Langmuir* **2010**, 26, 18331-18339.

(11) Lee, W. P.; Gundabala, V. R.; Akpa, B. S.; Johns, M. L.; Jeynes, C.; Routh, A. F. Distribution of Surfactants in Latex Films: A Rutherford Backscattering Study. *Langmuir* **2006**, 22, 5314-5320.

(12) Trueman, R. E.; Lago Domingues, E.; Emmett, S. N.; Murray, M. W.; Keddie, J. L.; Routh, A. F. Autostratification in Drying Colloidal Dispersions: Experimental Investigations. *Langmuir* **2012**, 28, 3420-3428.

(13) Nikiforow, I.; Adams, J.; König, A. M.; Langhoff, A.; Pohl, K.; Turshatov, A.; Johannsmann, D. Self-Stratification During Film Formation from Latex Blends Driven by Differences in Collective Diffusivity. *Langmuir* **2010**, 26, 13162-13167.

(14) Cima, M. J.; Lewis, J. A.; Devoe, A. D. Binder Distribution in Ceramic Greenware during Thermolysis. *J. Am. Ceram. Soc.* **1989**, 72, 1192-1199.

(15) Engström, G.; Rigdahl, M.; Kline, J.; Ahlroos, J. Binder Distribution and Mass Distribution of the Coating Layer - Cause and Consequence. *Tappi J.* **1991**, 74, 171-179.

(16) Kline, J. E. Measuring Binder Migration with Ultraviolet Analysis. *Tappi J.* **1991**, 74, 177-182.

(17) Luo, H.; Cardinal, C. M.; Scriven, L. E.; Francis, L. F. Ceramic Nanoparticle/Monodisperse Latex Coatings. *Langmuir* **2008**, 24, 5552-5561.

(18) Ma, Y.; Davis, H. T.; Scriven, L. E. Microstructure Development in Drying Latex Coatings. *Prog. Org. Coat.* **2005**, 52, 46-62.

(19) Stamou, D.; Duschl, C.; Johannsmann, D. Long-Range Attraction between Colloidal Spheres at the Air-Water Interface: The Consequence of an Irregular Meniscus. *Phys. Rev. E* **2000**, 62, 5263-5272.

(20) Cardinal, C. M.; Jung, Y. D.; Ahn, K. H.; Francis, L. F. Drying Regime Maps for Particulate Coatings. *AIChE J.* **2010**, 56, 2769-2780.

(21) Buss, F.; Roberts, C. C.; Crawford, K. S.; Peters, K.; Francis, L. F. Effect of Soluble Polymer Binder on Particle Distribution in a Drying Particulate Coating. *J. Colloid Interface Sci.* **2011**, 359, 112-120.

(22) Routh, A. F.; Zimmerman, W. B. Distribution of Particles during Solvent Evaporation from Films. *Chem. Eng. Sci.* **2004**, 59, 2961-2968.

(23) Yamamura, M. In-situ Characterization of Drying Particulate Coatings. *Kona Powder Particle J.* **2011**, No. 29, 39-52.

(24) Fergus, J. W. Recent Developments in Cathode Materials for Lithium Ion Batteries. *J. Power Sources* **2010**, 195, 939-954.

(25) Li, C. C.; Lee, J. T.; Peng, X. W. Improvements of Dispersion Homogeneity and Cell Performance of Aqueous-Processed $LiCoO_2$ Cathodes by Using Dispersant of PAA-NH_4. *J. Electrochem. Soc.* **2006**, 153, A809-A815.

(26) Lee, G. W.; Ryu, J. H.; Han, W.; Ahn, K. H.; Oh, S. M. Effect of Slurry Preparation Process on Electrochemical Performances of $LiCoO_2$ Composite Electrode. *J. Power Sources* **2010**, 195, 6049-6054.

(27) Lee, J. H.; Paik, U.; Hackley, V. A.; Choi, Y. M. Effect of Poly(acrylic acid) on Adhesion Strength and Electrochemical Performance of Natural Graphite Negative Electrode for Lithium-ion Batteries. *J. Power Sources* **2006**, 161, 612-616.

(28) Kajiya, T.; Kaneko, D.; Doi, M. Dynamical Visualization of "Coffee Stain Phenomenon" in Droplets of Polymer Solution via Fluorescent Microscopy. *Langmuir* **2008**, 24, 12369-12374.

(29) Ciddor, P. E. Refractive Index of Air: New Equations for the Visible and Near Infrared. *Appl. Opt.* **1996**, 35, 1566-1573.

(30) Schiebener, P.; Straub, J.; Levelt Sengers, J. M. H.; Gallagher, J. S. Refractive Index of Water and Steam as Function of Wavelength, Temperature and Density. *J. Phys. Chem. Ref. Data* **1990**, 19, 677-717.

(31) Kasarova, S. N.; Sultanova, N. G.; Ivanov, C. D.; Nikolov, I. D. Analysis of the Dispersion of Optical Plastic Materials. *Opt. Mater.* **2007**, 29, 1481-1490.

(32) Kiennemann, J.; Chartier, T.; Pagnoux, C.; Baumard, J. F.; Huger, M.; Lamérant, J. M. Drying Mechanisms and Stress Development in Aqueous Alumina Tape Casting. *J. Eur. Ceram. Soc.* **2005**, 25, 1551-1564.

(33) Weitz, D. A.; Zhu, J. X.; Durian, D. J.; Gang, H.;l Pine, D. J. Diffusing-Wave Spectroscopy: The Technique and Some Applications, *Physica Scripta* **1993**, 49, 610-621.

(34) Mason, T. G.; Gang, H.; Weitz, D. A. Diffusion-Wave-Spectroscopy measurements of Viscoelasticity of Complex Fluids, *J. Opt. Soc. Am. A* **1997**, 14, 139-149.

(35) Brun, A.; Dihang, H.; Brunel, L. Film Formation of Coatings Studied by Diffusing-Wave Spectroscopy, *Prog. Org. Coat.* **2008**, 61, 181-191.

(36) Faccia, P. A.; Pardini, O. R.; Amalvy, J. I.; Cap, N.; Grumel E. E.; Arizaga, R.; Trivi M. Differentiation of the Drying Time of Paints by Dynamic Speckle Interfereometry, *Prog. Org. Coat.* **2009**, 64, 350-355.

(37) Hermans, J., Jr. Investigation of Elastic Properties of Particle Network in Gelled Solutions of Hydrocolloids. I. Carboxymethyl Cellulose. *J. Polym. Sci. Polym. Chem.* **1965**, 3, 1859-1868.

(38) Kästner, U.; Hoffmann, H.; Dönges, R.; Hilbig, J. Structure and Solution Properties of Sodium Carboxymethyl Cellulose. *Colloids Surf., A* **1997**, 123-124, 307-328.

(39) Castelain, C.; Doublier, J. L.; Lefebvre, J. A Study of the Viscosity of Cellulose Derivatives in Aqueous Solutions. *Carbohyd. Polym.* **1987**, 7, 1-16.

(40) Gupta, P.; Elkins, C.; Long, T. E.; Wilkes, G. L. Electrospinning of Linear Homopolymers of Poly(methyl methacrylate): Exploring Relationships between Fiber Formation, Viscosity, Molecular Weight and Concentration in a Good Solvent. *Polymer* **2005**, 46, 4799-4810.

(41) Graessley, W. W. Polymer Chain Dimensions and the Dependence of Viscoelastic Properties on Concentration, Molecular Weight and Solvent Power. *Polymer* **1980**, 21, 258-262.

(42) Huggins, M. L. The Viscosity of Dilute Solutions of Long-Chain Molecules. IV. Dependence on Concentration. *J. Am. Chem. Soc.* **1942**, 64, 2716-2718

(43) Kraemer, E. O. Molecular Weights of Celluloses and Cellulose Derivatives. *Ind. Eng. Chem.* **1938**, 30, 1200-1203.

(44) Kurata, M.; Tsunashima, Y. Viscosity-Molecular Weight Relationships and Unperturbed Dimensions of Linear Chain Molecules. In *Polymer handbook*, 4th Edition; Brandrup, J.; Immergut, E. H.; Grulke, E. A.,Eds.; John Wiley & Sons, Inc.: New York, **1999**; pp VII1-83.

(45) Colby, R. H.; Rubinstein, M. Two-Parameter Scaling for Polymers in θ Solvents. *Macromolecules* **1990**, 23, 2753-2757.

(46) Colby, R. H.; Fetters, L. J.; Funk, W. G.; Graessley, W. W. Effects of Concentration and Thermodynamics Interaction on the Viscoelastic Properties of Polymer Solutions. *Macromolecules* **1991**, 24, 3873-3882.

(47) Colby, R. H.; Rubinstein, M.; Daoud, M. Hydrodynamics of Polymer Solutions *via* Two-Parameter Scaling. *J. Phys. II France* **1994**, 4, 1299-1310.

(48) Hamada, H.; Enomae, T.; Shibata, I.; Isogai, A.; Onabe, F. In *Effects of Water-Soluble Cellulose Polymers on Coating Development and Quality*, Proceedings of PITA Coating Conference, Edinburgh, Great Britain, March 4-5, 2003; Edinburgh, Great Britain, March 4-5, **2003**; pp 91-95.

(49) Bajpai, A. K.; Mishra, A. Ionizable Interpenetrating Polymer Networks of Carboxymethyl Cellulose and Polyacrylic Acid: Evaluation of Water Uptake. *J. Appl. Polym. Sci.* **2004**, 93, 2054-2065.

(50) Kim, S.; Sung, J. H.; Ahn, K. H.; Lee, S. J. Drying of the Silica/PVA Suspension: Effect of Suspension Microstructure. *Langmuir* **2009**, 25, 6155-6161.

(51) Kim, S.; Sung, J. H.; Chun, S.; Ahn, K. H.; Lee, S. J. Adsorption-Stress Relationship in Drying of Silica/PVA Suspensions. *J. Colloid Interface Sci.* **2011**, 361, 497-502.

(52) Pawlik, M.; Laskowski, J. S.; Ansari, A. Effect of Carboxymethyl Cellulose and Ionic Strength on Stability of Mineral Suspensions in Potash Ore Flotation Systems. *J. Colloid Interface Sci.* **2003**, 260, 251-258.

(53) Horigome, M.; Otsubo, Y. Long-Time Relaxation of Suspensions Flocculated by Associating Polymers. *Langmuir* **2002**, 18, 1968-1973.

(54) Pickrahn, K.; Rajaram, B.; Mohraz, A. Relationship between Microstructure, Dynamics, and Rheology in Polymer-Bridging Colloidal Gels. *Langmuir* **2009**, 26, 2392-2400.

(55) Runkana, V.; Somasundaran, P.; Kapur, P. C. A Population Balance Model for Flocculation of Colloidal Suspensions by Polymer Bridging. *Chem. Eng. Sci.* **2006**, 61, 182-191.

(56) Asakura, S.; Oosawa, F. Interaction between Particles Suspended in Solutions of Macromolecules. *J. Polym. Sci.* **1958**, 33, 183-192.

(57) Burns, J. L.; Yan, Y. D.; Jameson, G. J.; Biggs, S. The Effect of Molecular Weight of Nonadsorbing Polymer on the Structure of Depletion-Induced Flocs. *J. Colloid Interface Sci.* **2002**, 247, 24-32.

(58) Seebergh, J. E.; Berg, J. C. Depletion Flocculation of Aqueous, Electrosterically-Stabilized Latex Dispersions. *Langmuir* **1994**, 10, 454-463.

(59) Keddie, J. L.; Routh, A. F. An Introduction to Latex and the Principles of Colloidal Stability. In *Fundamentals of latex film formation: Processes and properties*, 1st Edition; Pasch, H.; Alig, I.; Janca, J.; Kulicke, W. -M., Eds.; Springer: Dordrecht, **2010**; pp 1-26.

FIGURES

Figure 1. (a) Schematic of drying apparatus, (b) image captured by CCD camera, (c) image captured by CCD beam profiler.

Figure 2. Dependence of intensity of fluorescent light on coating height and concentration of fluorescent particles: (a) intensity of fluorescent light plotted as a function of coating height for various concentrations of latex particles and (b) normalized intensity of fluorescent light plotted as a function of latex concentration for various coating heights.

Figure 3. Intensity of fluorescent light developed for latex-CMC suspension dried at various temperatures: (a) 0.5, (b) 1.0 wt% CMC solution and (c) divided regimes depending on the development of intensity of fluorescent light.

Figure 4. Development of beam spot during drying of 0.5 wt% CMC solution: (a) at initial drying, (b) at minimum size of beam spot, (c) at end of constant rate period, and (d) during final drying.

Figure 5. Development of beam spot during drying of 1.0 wt% CMC solution: (a) at initial drying, (b) at end of constant rate period, (c) during falling rate period, and (d) during final drying.

Figure 6. Development of intensity of fluorescent light emitted from graphite slurries at 70°C.

Figure 7. Images for 1 (a)–(c), and 5 wt% (d)–(f) graphite slurries: (a) and (d) are coating surfaces observed using optical microscope, (b) and (e) are coating surfaces observed using atomic force microscope, and (c) and (f) are cross-sections observed using SEM.

Figure 8. Development of intensity of fluorescent light emitted from 5 wt% graphite suspension depending on CMC concentration at various drying temperatures: (a) 0.5 and (b) 1.0 wt% CMC.

Figure 9. (a) ln η_{rel}/c and η_{sp}/c plotted as functions of CMC concentration. (b) log-log plot of zero-shear viscosity plotted as function of CMC concentration.

Figure 10. Isotherms for CMC adsorption onto surface of graphite particles, plotted as function of CMC concentration and ratio of CMC/graphite (graphite concentration was 5 wt%).

Figure 11. Sedimentation behavior of graphite slurries depending on concentration of CMC. (a) 5 wt% graphite slurry (ratio of CMC/graphite varied from 0 to 0.2) and (b) 1 wt% graphite slurry containing 0.7 wt% CMC (ratio of CMC/graphite is 0.7).

Figure 12. Critical development of intensity of fluorescent light emitted from graphite-free suspension (○) and 5 wt% graphite slurry (△) plotted as functions of CMC concentration at 30°C of drying temperature: (a) minimum, (b) maximum, and (c) final intensity of fluorescent light.

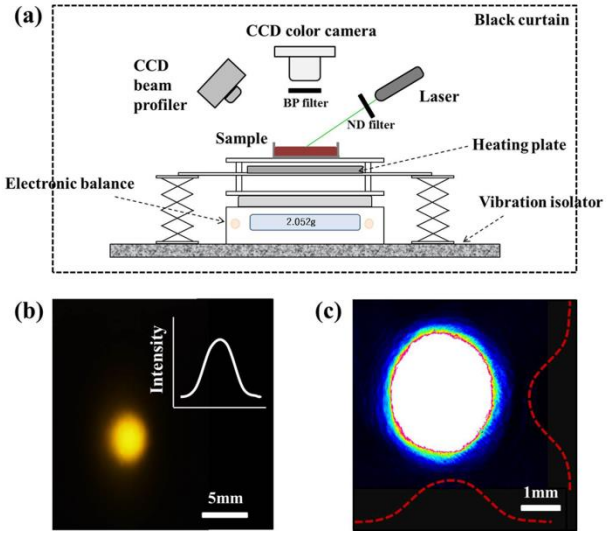

Figure 1. (a) Schematic of drying apparatus, (b) image captured by CCD camera, (c) image captured by CCD beam profiler.

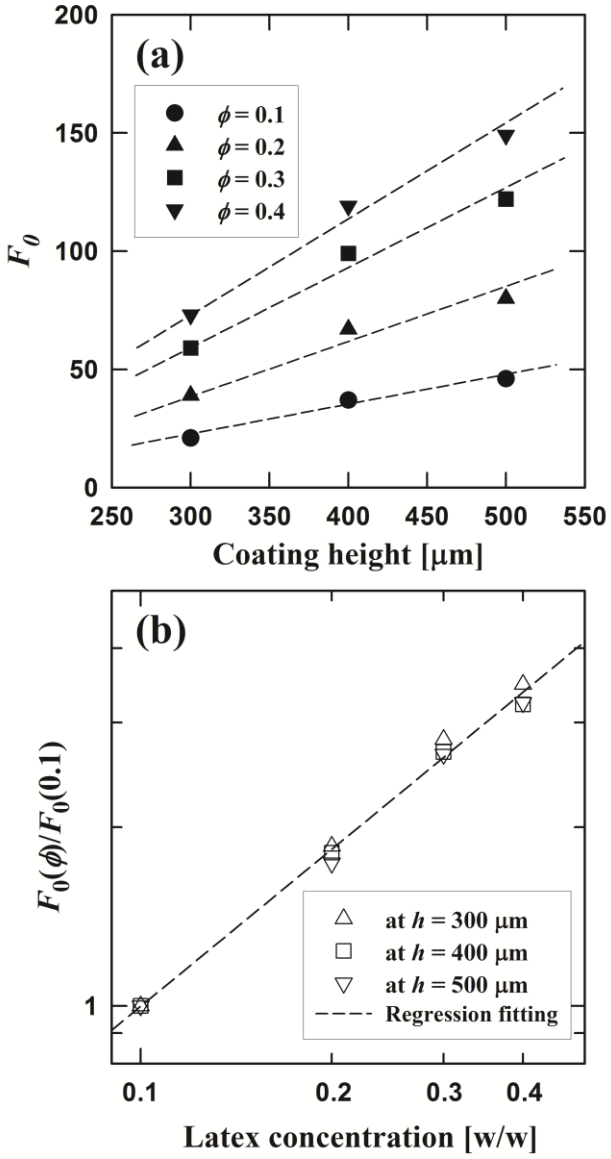

Figure 2. Dependence of intensity of fluorescent light on coating height and concentration of fluorescent particles: (a) intensity of fluorescent light plotted as a function of coating height for

various concentrations of latex particles and (b) normalized intensity of fluorescent light plotted as a function of latex concentration for various coating heights.

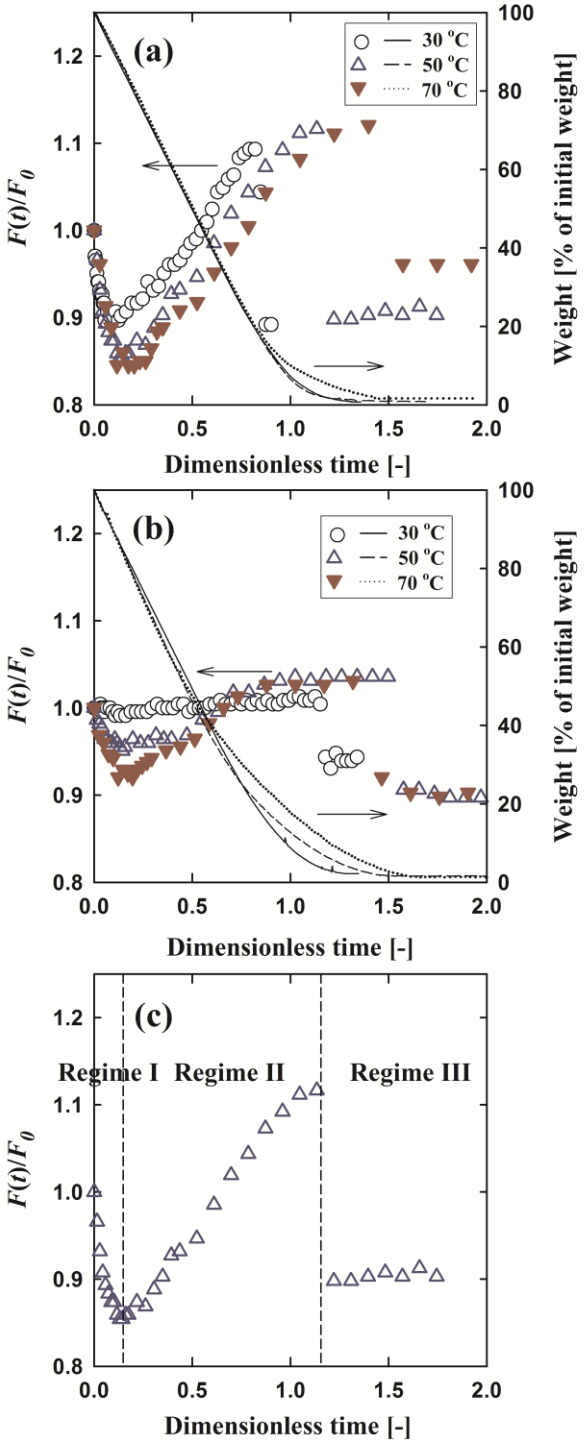

Figure 3. Intensity of fluorescent light developed for latex-CMC suspension dried at various temperatures: (a) 0.5, (b) 1.0 wt% CMC solution and (c) divided regimes depending on the development of intensity of fluorescent light.

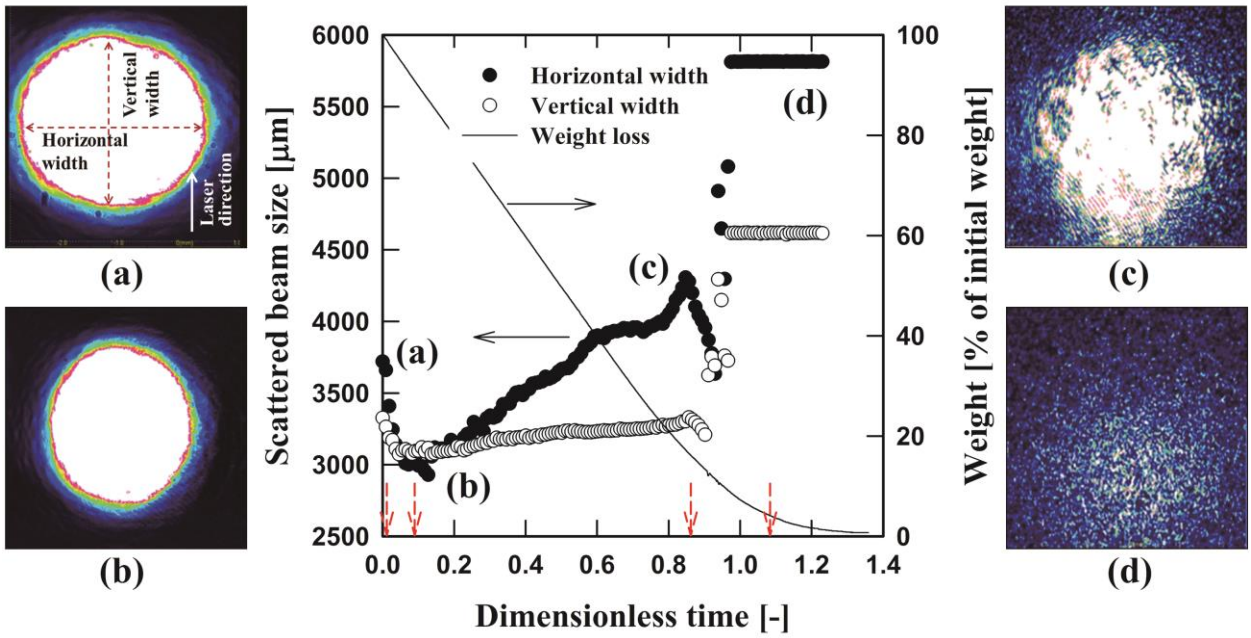

Figure 4. Development of beam spot during drying of 0.5 wt% CMC solution: (a) at initial drying, (b) at minimum size of beam spot, (c) at end of constant rate period, and (d) during final drying.

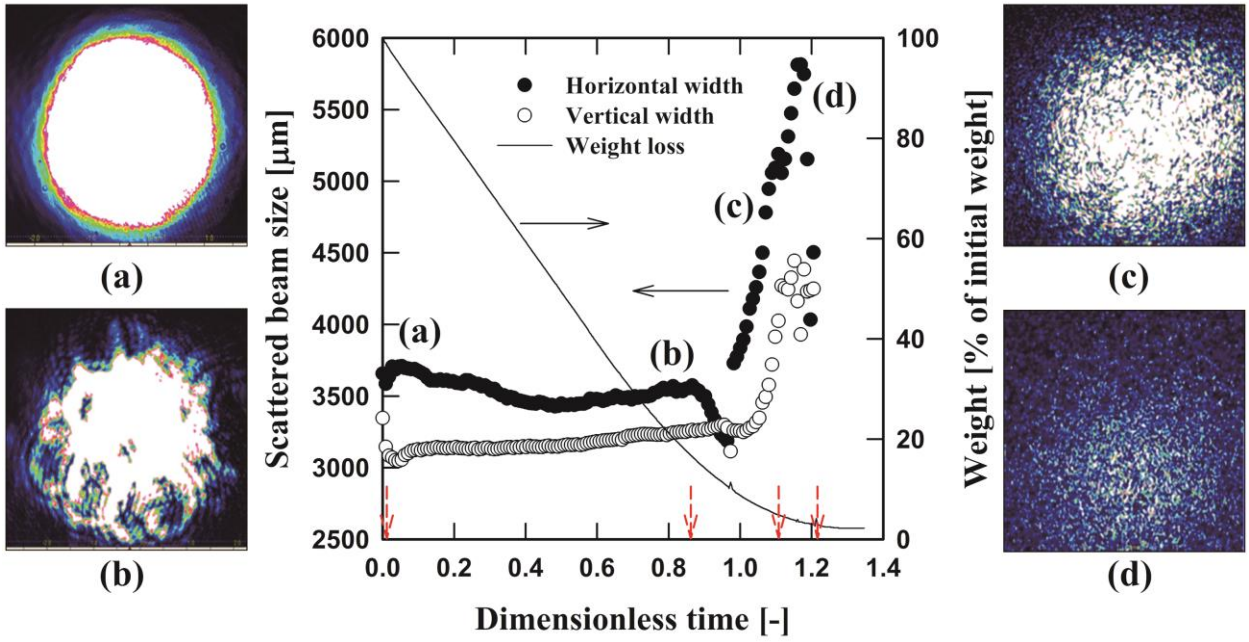

Figure 5. Development of beam spot during drying of 1.0 wt% CMC solution: (a) at initial drying, (b) at end of constant rate period, (c) during falling rate period, and (d) during final drying.

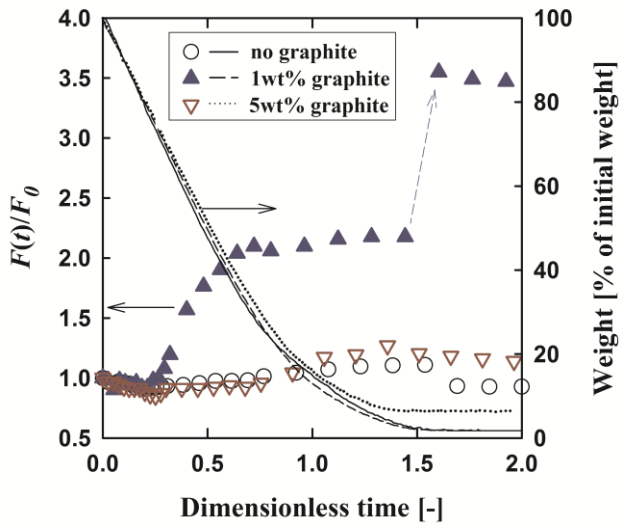

Figure 6. Development of intensity of fluorescent light emitted from graphite slurries at 70°C.

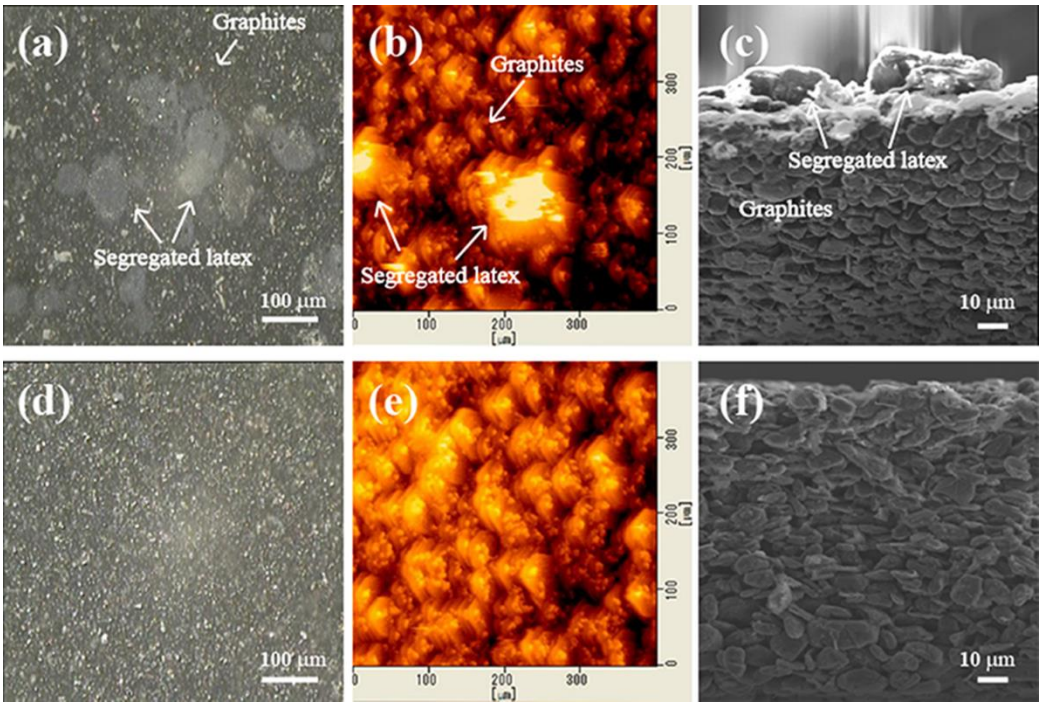

Figure 7. Images for 1 (a)–(c), and 5 wt% (d)–(f) graphite slurries: (a) and (d) are coating surfaces observed using optical microscope, (b) and (e) are coating surfaces observed using atomic force microscope, and (c) and (f) are cross-sections observed using SEM.

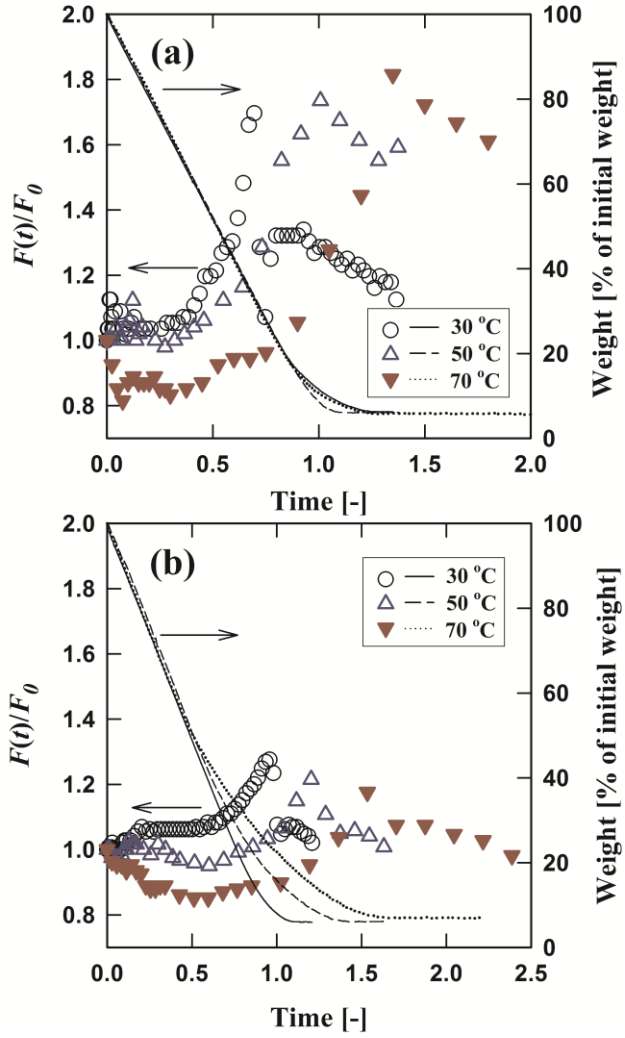

Figure 8. Development of intensity of fluorescent light emitted from 5 wt% graphite suspension depending on CMC concentration at various drying temperatures: (a) 0.5 and (b) 1.0 wt% CMC.

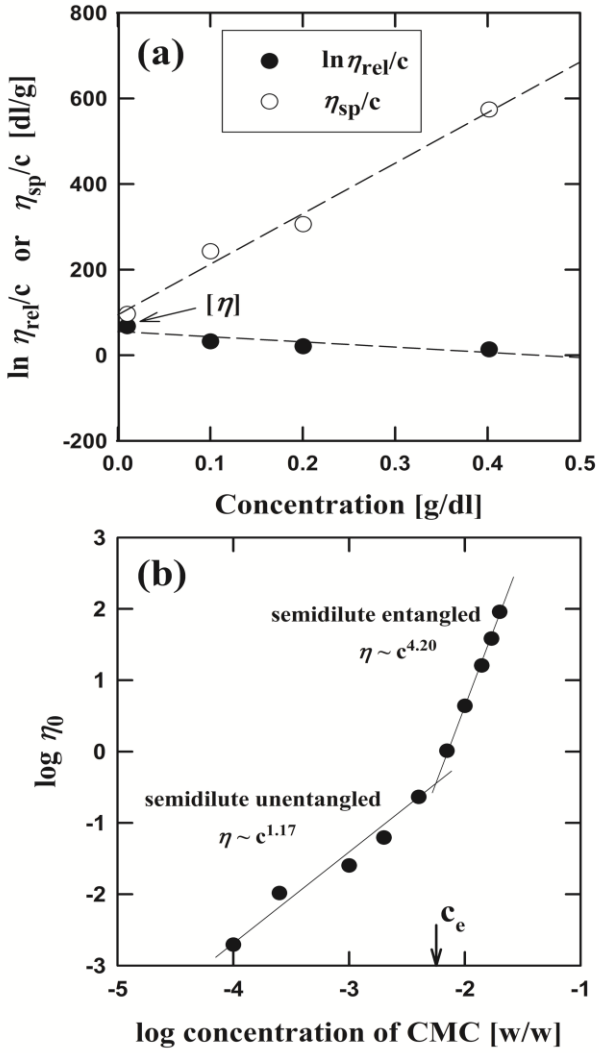

Figure 9. (a) ln η_{rel}/c and η_{sp}/c plotted as functions of CMC concentration. (b) log-log plot of zero-shear viscosity plotted as function of CMC concentration.

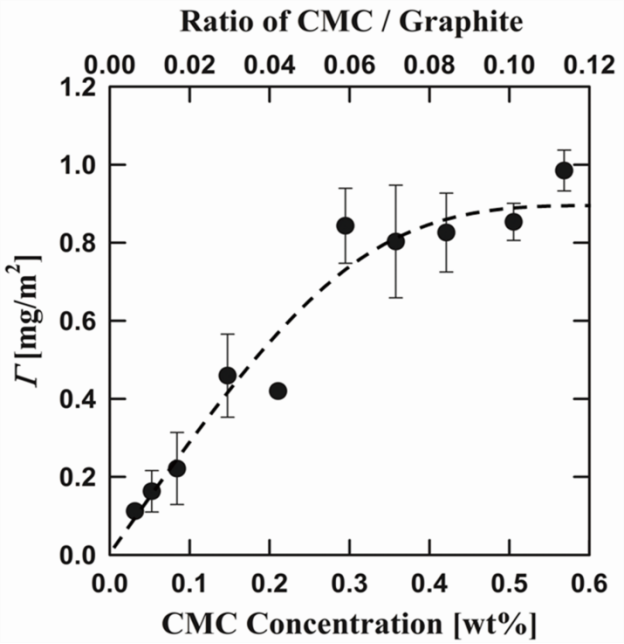

Figure 10. Isotherms for CMC adsorption onto surface of graphite particles, plotted as function of CMC concentration and ratio of CMC/graphite (graphite concentration was 5 wt%).

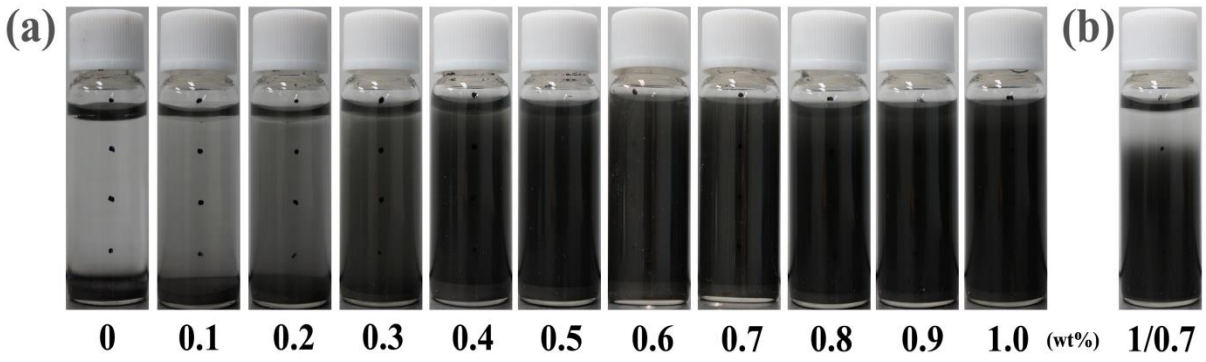

Figure 11. Sedimentation behavior of graphite slurries depending on concentration of CMC. (a) 5 wt% graphite slurry (ratio of CMC/graphite varied from 0 to 0.2) and (b) 1 wt% graphite slurry containing 0.7 wt% CMC (ratio of CMC/graphite is 0.7).

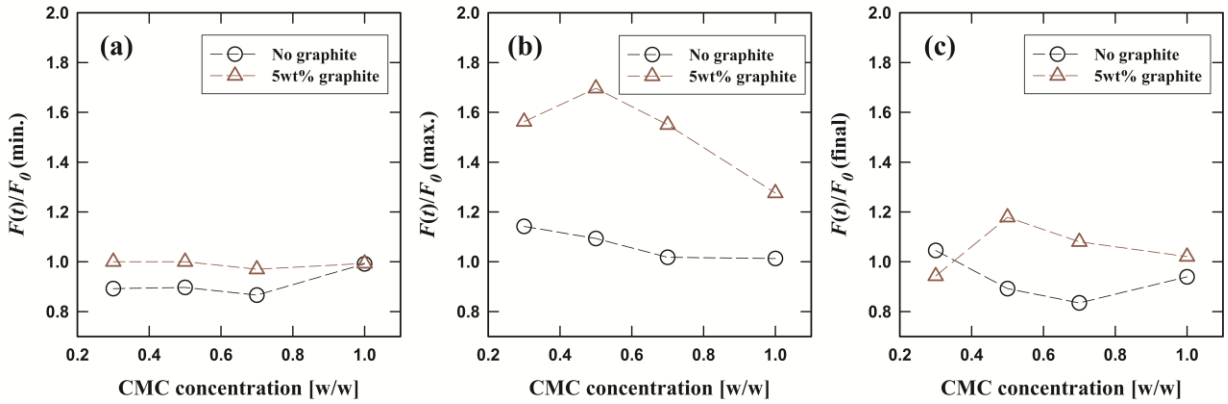

Figure 12. Critical development of intensity of fluorescent light emitted from graphite-free suspension (○) and 5 wt% graphite slurry (△) plotted as functions of CMC concentration at 30°C of drying temperature: (a) minimum, (b) maximum, and (c) final intensity of fluorescent light.

Table

Table 1. Constants and dimensionless numbers for latex particles in 0.5 wt% CMC solution.

Table 1. Constants and dimensionless numbers for latex particles in 0.5 wt% CMC solution.

Drying Temperature	μ (Pa·s)	E (m/s)	D_0 (m^2/s)	U_0 (m/s)	Pe	N_s
30°C	0.31	1.14×10^{-7}	1.41×10^{-14}	6.69×10^{-13}	4.05×10^{3}	5.88×10^{-6}
70°C	0.09	7.28×10^{-7}	5.24×10^{-14}	2.20×10^{-12}	6.94×10^{3}	3.02×10^{-6}